

Spin-Orbit-Induced Magnetic Anisotropy for Impurities in Metallic Samples II. Finite Size Dependence in the Kondo Resistivity

O. Újsághy^a and A. Zawadowski^{a,b}

^a*Institute of Physics and Research Group of Hungarian Academy of Sciences, Technical
University of Budapest, H-1521 Budapest, Hungary*

^b*Research Institute for Solid State Physics, POB 49, H-1525 Budapest, Hungary*

(November 5, 2021)

Abstract

The electrical resistivity including the Kondo resistivity increase at low temperature is calculated for thin films of dilute magnetic alloys. Assuming that in the non-magnetic host the spin-orbit interaction is strong like in Au and Cu, the magnetic impurities have a surface anisotropy calculated in part I. That anisotropy hinders the motion of the spin. Including that anisotropy the effective electron-impurity coupling is calculated by using the second order renormalization group equations. The amplitude of the Kondo resistivity contribution is reduced as the position of the impurity approaches the surface but the increase occurs approximately at the bulk Kondo temperature. Different proximity effects observed by Giordano are also explained qualitatively where the films of magnetic alloys are covered by pure second films with different mean free path. The theory explains the experimental results in those cases where a considerable amount of impurities is at the surface inside the

ballistic region.

PACS numbers: 72.15.Q, 73.50.M, 71.70.E

I. INTRODUCTION

In the previous paper [1] (Part I) following Ref's [2] and [3] we have calculated the magnetic anisotropy for a magnetic impurity embodied into a non-magnetic host (e.g. Au, Cu) with large spin-orbit interaction for the conduction electrons on the sites of the host atoms. The magnetic anisotropy is developed due to the exchange interaction between the magnetic impurities and the conduction electrons. As the scattering due to impurities involves different angular momentum channels ($-l < m < l$), therefore, the scattering depends on the directions of the conduction electrons before and after the scattering. In that way the scattering on the impurity itself depends on which host atoms the electrons are scattered by the spin-orbit interaction. Due to that dependence the anisotropy is determined by the positions of host atoms around the impurity and it is the larger the stronger the asymmetry around the impurity. As that information is carried by the momenta, therefore, that is restricted to the atoms in the range of the elastic mean free path l_{el} . Thus the anisotropy can be developed only if the impurity is inside surface area of the thickness of the elastic mean free path (ballistic region of the surface). If the surface in that region is plane like then the anisotropy energy is (see Eq. (1) of Part I [1])

$$H_a = K_d(\mathbf{n}\mathbf{S})^2, \tag{1}$$

where \mathbf{S} is the spin operator of the impurity, \mathbf{n} is the normal direction of the experienced surface element, and K_d is the anisotropy constant depending apart from the oscillatory part like $1/d$ on the distance d , measured from the surface. Of course, if the ballistic region contains more sophisticated part of the surface, then the determination of the direction and amplitude of the anisotropy is a more complex task. The oscillatory part decays faster than $1/d$ approaching the bulk part of the sample (see Eq. (B20b) in Part I).

In the surface area the anisotropy energy leads to different splitting schema shown in Fig. 1, depending whether the spin S is integer or half-integer. In this way the spin very nearby the surface is freezing into a singlet or doublet considering the integer and half-integer case,

respectively. Thus at low enough temperature the spin shows no, or restricted dynamics. It is important to point out, that the states $m = \pm 1/2$ for $S = 5/2$ cannot be replaced by a doublet of $S = 1/2$. The spins are rather squeezed into planar states as shown in Fig. 2.

Assuming that $K_d \gg T$, the integer spin does not contribute to the resistivity in contrary with the case of the half-integer spin where the two lowest states contribute to the resistivity. The spin $S = 1/2$ is, however, not affected by anisotropy. Thus different behaviors of the electrical resistivity can be expected depending on the value of the spin. Considering impurities nearby the surface inside the ballistic region more and more orbitals become active as the impurity positions approaching the bulk (see Fig. 3).

Similar structure appears in the temperature dependence of the resistivity. Cooling down the sample, at the beginning almost all the spins are free. At further cooling more and more spin states are frozen in thus in case $S = 2$ at $T < T_1$ three orbitals and $T < T_2$ a single orbital is populated ($T_1 : T_2 = 4 : 1$) while in case of $S = 5/2$ each state is double degenerate ($T_1 : T_2 = 25 : 9$).

Assuming that in the region of the Kondo temperature T_K the occupations of the different states are varying by considerable amount depending on the positions of the impurities in the surface region, then lowering the temperature less and less impurities can further develop the Kondo state, thus less and less impurities can contribute to further increase of the Kondo resistivity. As it has already been pointed out the reduction in the contribution to resistivity somewhat less pronounced for half-integer spin than for integer spin (see the discussion of Fig. 2). The contribution to the Kondo resistivity can be schematically plotted for impurities with different distances measured from the surface $d_3 < d_2 < d_1$ (see Fig. 4).

The phenomena described above are very similar to the Kondo effect in the presence of crystalline field at the impurity site when lowering the temperature different crystal field states are frozen out, but those fields are identical for all impurities of the same kind. Such calculations have been performed e.g. by Shin-ichi Kashiba *et al.* [4].

The reduction in the averaged Kondo resistivity is sensitive on the size of the sample e.g. film thickness or diameter of the wire etc. as the ratio of the surface influenced impurities to

the total number of the impurities goes to zero as the size is further increased. The role of the surface on the impurities can be reduced by depositing another pure film on the surface of the sample. The effect can be also influenced by changing the elastic mean free path in the samples or in the deposited films. The effects of those kinds will be summarized and discussed at the end of the paper (see Sec. VII) making use the qualitative results obtained for the resistivity in Sec. V and VI and all of the references can be found there.

For the actual calculation of the resistivity first the temperature dependence of the effective exchange coupling must be calculated. For that, except the very low temperature region, the second order multiplicative renormalization group transformations (two-loops approximation) can be used which give smooth behavior at the Kondo temperature in contrast to the first order scaling (one-loop approximation) which results in an artificial divergence at the Kondo temperature. Those methods are generalized by taking into account the surface anisotropy terms which occur as a low energy cutoff of the logarithmic integrals in the calculation of certain diagrams. The different diagrams depending on their spin labels have different infrared, low energy cutoff due to the anisotropy. These calculations are in close analogy to those with crystalline splitting. The next step is using these effective couplings to calculate the electrical resistivity by solving the Boltzmann equation and an average over the impurity positions is taken also.

Finally, to fit the calculated resistivity at low temperature, an effective surface layer thickness λ can be introduced, by assuming that inside of that surface region there is no Kondo effect, and outside the Kondo anomaly is fully developed. The experimental data are compared both with that phenomenological description and the original calculations and they are giving equally excellent fit.

The paper is organized as follows. In Sec. II the general scheme of the multiplicative renormalization group (MRG) is presented for the Hamiltonian with the anisotropy term. The scaling equations are presented in Sec. III which are solved in Sec. IV. The electrical resistivity contribution is calculated in Sec. V for the dilute limit and Kondo resistivity in thin films is given in Sec. VI. Sec. VII is devoted to the experimental results, theoretical

interpretation of the results and prediction. A general discussion is contained in Sec. VIII. The Appendix contains the actual calculation of the diagrams which are needed in Sec. III. Throughout the paper the $\hbar = k_B = 1$ units were used.

II. THE HAMILTONIAN AND THE GENERAL FORM OF THE MRG TRANSFORMATION

The Kondo Hamiltonian in the presence of the anisotropy is

$$H = \sum_{k,\sigma} \varepsilon_k a_{k\sigma}^\dagger a_{k\sigma} + H_a + \sum_{\substack{k,k',\sigma,\sigma' \\ M,M'}} J_{MM'} \mathbf{S}_{MM'} (a_{k\sigma}^\dagger \boldsymbol{\sigma}_{\sigma\sigma'} a_{k'\sigma'}), \quad (2)$$

where $a_{k\sigma}^\dagger$ ($a_{k\sigma}$) creates (annihilates) a conduction electron with momentum k , spin σ and energy ε_k measured from the Fermi level. The conduction electron band is taken with constant energy density ρ_0 for one spin direction, with a sharp and symmetric bandwidth cutoff D . $\boldsymbol{\sigma}$ stands for the Pauli matrices, $J_{MM'}$'s are the effective Kondo couplings and H_a is given by Eq. (1). For the impurity spin the Abrikosov' pseudofermion representation [5] was used

$$\mathbf{S} = b_M^\dagger \mathbf{S}_{MM'} b_{M'}, \quad (3)$$

where the projections of the z component of the impurity spin are described by an auxiliary fermionic field b_M ($M = -S \dots S$). Choosing the quantization axis parallel to \mathbf{n} , with this substitution the Hamiltonian Eq. (2) become

$$H = \sum_{k,\sigma} \varepsilon_k a_{k\sigma}^\dagger a_{k\sigma} + \sum_M (\lambda + K_M) b_M^\dagger b_M + \sum_{\substack{k,k',\sigma,\sigma' \\ M,M'}} J_{MM'} (b_M^\dagger \mathbf{S}_{MM'} b_{M'}) (a_{k\sigma}^\dagger \boldsymbol{\sigma}_{\sigma\sigma'} a_{k'\sigma'}), \quad (4)$$

where the chemical potential $\lambda \rightarrow \infty$ was introduced to project out the physical pseudofermion subspace $\sum_M b_M^\dagger b_M = 1$ and the notation $K_M = KM^2$ was introduced for the MRG calculation.

The conduction electron and pseudofermion Green's functions are

$$G_{k\sigma,k'\sigma'}(\omega) = \frac{\delta_{kk'}\delta_{\sigma\sigma'}}{\omega - \varepsilon_k - \Sigma_e} \quad (5)$$

and

$$\mathcal{G}_{MM'}(\tilde{\omega}) = \frac{\delta_{MM'}}{\tilde{\omega} - \lambda - \Sigma_M(\tilde{\omega})} \quad (6)$$

where $\tilde{\omega} = \omega - K_M$. Σ_e and $\Sigma_M(\tilde{\omega})$ are the self-energies for the conduction electrons and the pseudofermions, respectively. They are diagonal in the adequate spin quantum numbers, because of that the whole Hamiltonian is symmetric under rotation around the z axis. The vertex function is denoted by $\Gamma_{k\sigma M,k'\sigma' M'}(\omega_1, \omega_2, \omega_3, \omega_4)$.

The multiplicative renormalization group transformation can be written as [6]

$$G_{k\sigma,k'\sigma'}(\omega, J_{MM'}(D), K_M(D), D) = Z\left(\frac{D_0}{D}\right) G_{k\sigma,k'\sigma'}(\omega, J_{MM'}^0, K_M^0, D_0) \quad (7a)$$

$$\mathcal{G}_{MM'}(\tilde{\omega}, J_{\tilde{M}\tilde{M}'}(D), K_{\tilde{M}}(D), D) = Z_M\left(\frac{D_0}{D}\right) \mathcal{G}_{MM'}(\tilde{\omega}, J_{\tilde{M}\tilde{M}'}^0, K_{\tilde{M}}^0, D_0) \quad (7b)$$

$$\Gamma_{k\sigma M,k'\sigma' M'}(\omega_i, J_{\tilde{M}\tilde{M}'}(D), K_{\tilde{M}}(D), D) = \frac{\Gamma_{k\sigma M,k'\sigma' M'}(\omega_i, J_{\tilde{M}\tilde{M}'}^0, K_{\tilde{M}}^0, D_0)}{Z(\frac{D_0}{D})\sqrt{Z_M(\frac{D_0}{D})}\sqrt{Z_{M'}(\frac{D_0}{D})}}, \quad (7c)$$

where $Z(\frac{D_0}{D})$ and $Z_M(\frac{D_0}{D})$ are the renormalization factors for the electrons and pseudofermions, respectively. Introducing $x = \ln(\frac{D_0}{D})$ as scaling parameter, the Callan-Symantzik MRG equations are

$$-\eta G + \frac{\partial G}{\partial x} + \sum_{MM'} \beta_{MM'} \frac{\partial G}{\partial J_{MM'}} + \sum_M \gamma_M \frac{\partial G}{\partial K_M} = 0 \quad (8a)$$

$$-\eta_M \mathcal{G}_M + \frac{\partial \mathcal{G}_M}{\partial x} + \sum_{\tilde{M}\tilde{M}'} \beta_{\tilde{M}\tilde{M}'} \frac{\partial \mathcal{G}_M}{\partial J_{\tilde{M}\tilde{M}'}} + \sum_{\tilde{M}} \gamma_{\tilde{M}} \frac{\partial \mathcal{G}_M}{\partial K_{\tilde{M}}} = 0 \quad (8b)$$

$$(\eta + \frac{1}{2}\eta_M + \frac{1}{2}\eta_{M'})\Gamma_{MM'} + \frac{\partial \Gamma_{MM'}}{\partial x} + \sum_{\tilde{M}\tilde{M}'} \beta_{\tilde{M}\tilde{M}'} \frac{\partial \Gamma_{MM'}}{\partial J_{\tilde{M}\tilde{M}'}} + \sum_{\tilde{M}} \gamma_{\tilde{M}} \frac{\partial \Gamma_{MM'}}{\partial K_{\tilde{M}}} = 0, \quad (8c)$$

where

$$\eta = \frac{d \ln Z}{dx} \quad (9a)$$

$$\eta_M = \frac{d \ln Z_M}{dx} \quad (9b)$$

$$\beta_{MM'} = \frac{dJ_{MM'}}{dx} \quad (9c)$$

$$\gamma_M = \frac{dK_M}{dx} \quad (9d)$$

and for the sake of simplicity the electron and pseudofermion Green's function, and the vertex function were denoted by G , \mathcal{G}_M , and $\Gamma_{MM'}$, respectively. The initial values for the renormalization factors and couplings are $Z = Z_M = 1$, $K_M = K_M^{(0)} = KM^2$, $J_{MM'} = J_0$ for each M, M' , at $D = D_0$.

Using the definition of self energies in Eq. (5) and (6) the first two equations can be rewritten as

$$-(\omega - \varepsilon_k - \Sigma_e)\eta + \frac{\partial \Sigma_e}{\partial x} + \sum_{MM'} \beta_{MM'} \frac{\partial \Sigma_e}{\partial J_{MM'}} + \sum_M \gamma_M \frac{\partial \Sigma_e}{\partial K_M} = 0 \quad (10a)$$

$$-(\tilde{\omega} - \lambda - \Sigma_M)\eta_M + \frac{\partial \Sigma_M}{\partial x} + \sum_{\tilde{M}\tilde{M}'} \beta_{\tilde{M}\tilde{M}'} \frac{\partial \Sigma_M}{\partial J_{\tilde{M}\tilde{M}'}} + \sum_{\tilde{M}} \gamma_{\tilde{M}} \frac{\partial \Sigma_M}{\partial K_{\tilde{M}}} + \frac{dK_M}{dx} = 0 \quad (10b)$$

which form is more comfortable for calculating the MRG equations.

III. CONSTRUCTION OF THE MRG EQUATIONS

To construct the MRG equations the perturbation theory was applied, that is the Hamiltonian was divided into a non-interacting and an interaction part with small parameters $J_{MM'}$'s.

For which the electron self energy contains a closed pseudofermion loop, Σ_e tends to zero as $\lambda \rightarrow \infty$. Thus in the thermodynamical limit for a single impurity from Eq. (10a) $\eta = 0$ and $Z = 1$.

Turning to the other two equations Eq. (10b), (8c) they were solved in next to leading logarithmic approximation where the MRG equations are

$$(\tilde{\omega} - \lambda)\eta_M^{(2)} = \frac{\partial \delta \Sigma_M^{(2)}}{\partial x} + \gamma_M^{(2)} \quad (11)$$

and

$$\frac{\partial \delta \Gamma_{\sigma M, \sigma' M'}^{(2)}}{\partial x} + \sigma_{\sigma \sigma'} \mathbf{S}_{MM'} \beta_{MM'}^{(2)} = 0, \quad (12a)$$

$$\begin{aligned} & \left(\frac{1}{2} \eta_M^{(2)} + \frac{1}{2} \eta_{M'}^{(2)} \right) J_{MM'} \sigma_{\sigma \sigma'} \mathbf{S}_{MM'} + \frac{\partial \delta \Gamma_{\sigma M, \sigma' M'}^{(3)}}{\partial x} \\ & + \sum_{\tilde{M} \tilde{M}'} \beta_{\tilde{M} \tilde{M}'}^{(2)} \frac{\partial \Gamma_{\sigma M, \sigma' M'}^{(2)}}{\partial J_{\tilde{M} \tilde{M}'}} + \sigma_{\sigma \sigma'} \mathbf{S}_{MM'} \beta_{MM'}^{(3)} = 0 \end{aligned} \quad (12b)$$

where $\eta_M^{(2)}$, $\gamma_M^{(2)}$ and $\beta_{MM'}^{(2)}$ are proportional to the second, $\beta_{MM'}^{(3)}$ to the third power of the $J_{MM'}$'s, respectively. The whole next to leading logarithmic β -function is $\beta_{MM'} = \beta_{MM'}^{(2)} + \beta_{MM'}^{(3)}$.

Thus to construct the next to leading logarithmic scaling equations we have to calculate the second ($\delta \Gamma_{\sigma M, \sigma' M'}^{(2)}$) and third ($\delta \Gamma_{\sigma M, \sigma' M'}^{(3)}$) order vertex corrections, and the second order self energy correction ($\delta \Sigma_M^{(2)}$) for the impurity spin.

These corrections were calculated by applying the thermodynamical Green's function technique and analytical continuation [7]. Assuming scaling for the vertex function $\Gamma_{MM'}$ only one energy variable was kept [8], thus $\omega_1 = \omega$, $\omega_2 = K_M$, $\omega_3 = \omega + K_M - K_{M'}$ and $\omega_4 = K_{M'}$, where ω_1 , ω_2 the incoming, ω_3 , ω_4 the outgoing electron and pseudofermion energies, respectively.

The second and third order vertex diagrams, and the second order correction to the self-energy for the impurity spin are shown in Fig. 5 and Fig. 6, respectively. The detailed calculation of these diagrams is carried out in the Appendix. Collecting the whole second and third order vertex corrections together, they and the self-energy correction for the impurity spin were substituted into the Eq's (11) and (12). In Eq. (12b) the contributions of the third order parquet-type diagrams depicted in Fig. 5 (b) and (d) were canceled out with the

terms $\sum_{\tilde{M}\tilde{M}'} \beta_{\tilde{M}\tilde{M}'}^{(2)} \frac{\partial \Gamma_{\sigma_M, \sigma' M'}^{(2)}}{\partial J_{\tilde{M}\tilde{M}'}}$ as the leading logarithmic scaling equations are equivalent to the summing up of the parquet diagrams. The divergences at finite T were canceled out, too. Thus only the diagram Fig. 5 (c) contributes to Eq. (12b).

Introducing the dimensionless couplings $j_{MM'} = \rho_0 J_{MM'}$ the next to leading logarithmic scaling equations are

$$\eta_M = \frac{d \ln Z_M}{dx} = q^2(S, M) j_{M, M-1} j_{M-1, M} \Theta_{M, M-1}(D) + p^2(S, M) j_{M, M+1} j_{M+1, M} \Theta_{M, M+1}(D) + 2M^2 j_{M, M}^2 \quad (13)$$

$$\gamma_M = \frac{dK_M}{dx} = (K_{M-1} - K_M) q^2(S, M) j_{M, M-1} j_{M-1, M} \Theta_{M, M-1}(D) + (K_{M+1} - K_M) p^2(S, M) j_{M, M+1} j_{M+1, M} \Theta_{M, M+1}(D) \quad (14)$$

$$\begin{aligned} \rho_0 \beta_{M, M+1} &= \frac{dj_{M, M+1}}{dx} = -(M j_{M, M} - (M+1) j_{M+1, M+1}) j_{M, M+1} (1 + \Theta_{M, M+1}(D)) \\ &+ q^2(S, M) j_{M, M-1} j_{M-1, M} j_{M, M+1} \Theta_{M, M-1}(D) \left(\Theta_{M, M+1}(D) - \frac{1}{2} \right) \\ &+ p^2(S, M+1) j_{M, M+1} j_{M+1, M+2} j_{M+2, M+1} \Theta_{M+1, M+2}(D) \left(\Theta_{M, M+1}(D) - \frac{1}{2} \right) \\ &- p^2(S, M) j_{M, M+1}^2 j_{M+1, M} \Theta_{M, M+1}(D) - M^2 j_{M, M}^2 j_{M, M+1} \\ &- (M+1)^2 j_{M+1, M+1}^2 j_{M, M+1} + 2M(M+1) j_{M, M} j_{M, M+1} j_{M+1, M+1} \end{aligned} \quad (15)$$

$$\begin{aligned} \rho_0 \beta_{M, M-1} &= \frac{dj_{M, M-1}}{dx} = -((M-1) j_{M-1, M-1} - M j_{M, M}) j_{M, M-1} (1 + \Theta_{M, M-1}(D)) \\ &+ p^2(S, M) j_{M, M+1} j_{M+1, M} j_{M, M-1} \Theta_{M, M+1}(D) \left(\Theta_{M, M-1}(D) - \frac{1}{2} \right) \\ &+ q^2(S, M-1) j_{M, M-1} j_{M-1, M-2} j_{M-2, M-1} \Theta_{M-1, M-2}(D) \left(\Theta_{M, M-1}(D) - \frac{1}{2} \right) \\ &- q^2(S, M) j_{M, M-1}^2 j_{M-1, M} \Theta_{M, M-1}(D) - M^2 j_{M, M}^2 j_{M, M-1} \\ &- (M-1)^2 j_{M-1, M-1}^2 j_{M, M-1} + 2M(M-1) j_{M, M} j_{M, M-1} j_{M-1, M-1} \end{aligned} \quad (16)$$

and for $M \neq 0$

$$\begin{aligned} \rho_0 \beta_{M, M} &= \frac{dj_{M, M}}{dx} \\ &= \frac{1}{M} \left[q^2(S, M) \Theta_{M, M-1}(D) j_{M, M-1} j_{M-1, M} - p^2(S, M) \Theta_{M, M+1}(D) j_{M, M+1} j_{M+1, M} \right] \end{aligned}$$

$$\begin{aligned}
& + q^2(S, M) \frac{M-1}{M} j_{M,M-1} j_{M-1,M-1} j_{M-1,M} \Theta_{M,M-1}(D) \\
& + p^2(S, M) \frac{M+1}{M} j_{M,M+1} j_{M+1,M+1} j_{M+1,M} \Theta_{M,M+1}(D) \\
& - q^2(S, M) j_{M,M-1} j_{M-1,M} j_{M,M} \Theta_{M,M-1}(D) \\
& - p^2(S, M) j_{M,M+1} j_{M+1,M} j_{M,M} \Theta_{M,M+1}(D)
\end{aligned} \tag{17}$$

where $\Theta_{MM'}(D)$ ensures that $D > \sqrt{(K_M - K_{M'})^2 + T^2}$ with the definition

$$\Theta_{MM'}(D) = \begin{cases} 1 & \text{if } D > \sqrt{(K_M - K_{M'})^2 + T^2} \\ 0 & \text{if } D < \sqrt{(K_M - K_{M'})^2 + T^2}. \end{cases} \tag{18}$$

The definition of $p(S, M)$ and $q(S, M)$ are given in Eq. (A7). It must be stressed that these scaling equations are valid for $T \leq D$.

IV. SOLUTION OF THE SCALING EQUATIONS

It can be seen from Eq. (14), that the corrections to the bare $K_M^{(0)}$ are proportional to the second power of $j_{MM'}$'s in the leading order. In the other equations K_M appears only in the arguments of the Θ functions which are multiplied by the second or third power of $J_{MM'}$'s. Thus to keep in the approximation consistent $K_M = K_M^{(0)} = KM^2$ can be taken in the arguments of the Θ functions. After this consideration the solution of the equations becomes simpler, because the equations for $\beta_{MM'}$ are not coupled. Exploiting the symmetries of the scaling equations

$$j_{M,M'} = j_{M',M} \tag{19a}$$

$$j_{M,M'} = j_{-M,-M'} \tag{19b}$$

must hold.

Thus the equations which have to be solved are

$$\frac{dj_{M,M+1}}{dx} = -(Mj_{M,M} - (M+1)j_{M+1,M+1})j_{M,M+1}(1 + \Theta_{M,M+1}(D))$$

$$\begin{aligned}
& + q^2(S, M)j_{M,M-1}^2 j_{M,M+1} \Theta_{M,M-1}(D) \left(\Theta_{M,M+1}(D) - \frac{1}{2} \right) \\
& + p^2(S, M+1)j_{M,M+1} j_{M+1,M+2}^2 \Theta_{M+1,M+2}(D) \left(\Theta_{M,M+1}(D) - \frac{1}{2} \right) \\
& - p^2(S, M)j_{M,M+1}^3 \Theta_{M,M+1}(D) - M^2 j_{M,M}^2 j_{M,M+1} \\
& - (M+1)^2 j_{M+1,M+1}^2 j_{M,M+1} + 2M(M+1)j_{M,M} j_{M,M+1} j_{M+1,M+1}
\end{aligned} \tag{20}$$

and for $M \neq 0$

$$\begin{aligned}
\frac{dj_{M,M}}{dx} = \frac{1}{M} & \left[q^2(S, M) \Theta_{M,M-1}(D) j_{M,M-1}^2 \right. \\
& \left. - p^2(S, M) \Theta_{M,M+1}(D) j_{M,M+1}^2 \right] \\
& + q^2(S, M) \frac{M-1}{M} j_{M,M-1}^2 j_{M-1,M-1} \Theta_{M,M-1}(D) \\
& + p^2(S, M) \frac{M+1}{M} j_{M,M+1}^2 j_{M+1,M+1} \Theta_{M,M+1}(D) \\
& - q^2(S, M) j_{M,M-1}^2 j_{M,M} \Theta_{M,M-1}(D) \\
& - p^2(S, M) j_{M,M+1}^2 j_{M,M} \Theta_{M,M+1}(D)
\end{aligned} \tag{21}$$

These equations were solved numerically for different initial couplings $j_0 = j_{MM'}(D = D_0)$. The results for $j_0 = 0.1$ and $j_0 = 0.0435$ at $K/T = 10$ are shown in Fig. 7 and Fig. 8 for $S = 2$ and $S = 5/2$, respectively. The initial bandwidth cutoff was chosen as $D_0 = 10^5$ K.

V. RESISTIVITY

The Kondo resistivity was calculated by solving the Boltzmann equation in the presence of the spin-orbit induced anisotropy, using the value of running couplings ($j_{MM'}$) calculated in the preceding section, at $D = T$.

Taking the usual form [9] for the electron distribution function $f(\varepsilon_k)$ in the presence of the electric field \mathbf{E} as

$$f(\varepsilon_k) = f_0(\varepsilon_k) - (\mathbf{k}\mathbf{E})\Phi(\varepsilon_k) \frac{\partial f_0(\varepsilon_k)}{\partial \varepsilon_k}, \tag{22}$$

the Kondo contribution to the resistivity is

$$\frac{1}{\rho_{\text{Kondo}}} = -\frac{e}{3\pi^2}(2m)^{3/2} \int d\varepsilon_k \varepsilon_k^{3/2} \Phi(\varepsilon_k) \left(-\frac{\partial f_0}{\partial \varepsilon_k} \right) \quad (23)$$

where the function Φ is determined by the Boltzmann equation

$$\frac{e}{m} \frac{\partial f_0(\varepsilon_k)}{\partial \varepsilon_k}(\mathbf{k}\mathbf{E}) + \left(\frac{\partial f}{\partial t} \right)_{\text{coll.}} = 0. \quad (24)$$

The collision term $(\frac{\partial f}{\partial t})_{\text{coll.}}$ can be expressed in terms of transition probabilities as

$$\begin{aligned} \left(\frac{\partial f}{\partial t} \right)_{\text{coll.}} &= \frac{c}{V} \sum_{\mathbf{k}'\sigma'} \{ W(\mathbf{k}', \sigma' \rightarrow \mathbf{k}, \sigma) f(\mathbf{k}') (1 - f(\mathbf{k})) \\ &\quad - W(\mathbf{k}, \sigma \rightarrow \mathbf{k}', \sigma') f(\mathbf{k}) (1 - f(\mathbf{k}')) \} \end{aligned} \quad (25)$$

where e.g. $W(\mathbf{k}', \sigma' \rightarrow \mathbf{k}, \sigma)$ represents the transition probability from a \mathbf{k}', σ' state to a \mathbf{k}, σ , c is the impurity concentration, and V is the volume.

Turning to our case, these probabilities can be calculated as

$$W(\mathbf{k}, \sigma \rightarrow \mathbf{k}', \sigma') = \sum_{MM'} p_M w(\mathbf{k}, \sigma, M \rightarrow \mathbf{k}', \sigma', M') \quad (26)$$

where

$$w(\mathbf{k}, \sigma, M \rightarrow \mathbf{k}', \sigma', M') = 2\pi |T_{\mathbf{k}, \sigma, M \rightarrow \mathbf{k}', \sigma', M'}|^2 \delta(\varepsilon_k - \varepsilon_{k'} + KM^2 - KM'^2), \quad (27)$$

and $p_M = e^{-\beta KM^2}/Z$, $\beta = 1/T$, $Z = \sum_M e^{-\beta KM^2}$.

The scattering amplitude in Eq. (27) is expressed in terms of the renormalized couplings $J_{MM'}(x)$ as

$$T_{\mathbf{k}, \sigma, M \rightarrow \mathbf{k}', \sigma', M'} \approx J_{MM'}(x = \ln \frac{D_0}{T}) \boldsymbol{\sigma}_{\sigma\sigma'} \mathbf{S}_{MM'} \quad (28)$$

where the dependence on the direction of the momenta \mathbf{k} and \mathbf{k}' is ignored and that makes the Boltzmann equation solvable in a simple form. The \mathbf{k} -dependence may result as some numerical factors in the final expression, but in the main features of the temperature dependence those are not playing an important role.

Substituting these assumptions into Eq. (25), changing the sum $\frac{1}{V} \sum_{k'}$ to $\int \rho(\varepsilon_{k'}) d\varepsilon_{k'} \int \frac{d\Omega_{k'}}{4\pi} \approx \rho_0 \int_{-D_0}^{D_0} d\varepsilon \int \frac{d\Omega_{k'}}{4\pi}$, using the properties of the spin algebra for $\boldsymbol{\sigma}$ and \mathbf{S} and the "detailed balance" principle ($(\frac{\partial f_0(\varepsilon_k)}{\partial t})_{\text{coll.}} = 0$), we obtain after linearization in \mathbf{E}

$$\left(\frac{\partial f}{\partial t}\right)_{\text{coll.}} = \frac{2\pi c}{\rho_0}(\mathbf{k}\mathbf{E})\Phi(\varepsilon_k)\frac{\partial f_0}{\partial \varepsilon_k}F(\varepsilon_k) \quad (29)$$

where

$$\begin{aligned} F(\varepsilon_k) = \sum_M p_M \Big\{ & M^2 j_{M,M}^2(x = \ln \frac{D_0}{T}) \\ & + (S(S+1) - M(M+1))j_{M,M+1}^2(x = \ln \frac{D_0}{T}) \\ & \cdot [1 - (1 - e^{-(2M+1)K/T})f_0(\varepsilon_k - (2M+1)K)] \Big\} \end{aligned} \quad (30)$$

where we introduced the dimensionless coupling constants $j_{MM'} = \rho_0 J_{MM'}$. Inserting Eq. (29) into the Boltzmann Eq. (24) we obtain for Φ

$$\Phi(\varepsilon_k) = -\frac{e}{m} \left[\frac{2\pi c}{\rho_0} F(\varepsilon_k) \right]^{-1} \quad (31)$$

and for the Kondo resistivity

$$\frac{1}{\rho_{\text{Kondo}}} = \frac{1}{\rho^{(0)}} \int d\varepsilon \left(-\frac{\partial f_0}{\partial \varepsilon} \right) F^{-1}(\varepsilon) \quad (32)$$

where the usual assumption

$$\int d\varepsilon \varepsilon^{3/2} \left(-\frac{\partial f_0}{\partial \varepsilon} \right) F^{-1}(\varepsilon) \approx \varepsilon_F^{3/2} \int d\varepsilon \left(-\frac{\partial f_0}{\partial \varepsilon} \right) F^{-1}(\varepsilon) \quad (33)$$

was taken into account and the constant $\rho^{(0)} = \frac{3}{4} \frac{m}{e^2} \frac{2\pi c}{\varepsilon_F \rho_0^2}$ was introduced.

In the case of $K = 0$, Eq. (32) reproduces the bulk Kondo resistivity.

The resistivity was calculated by evaluating the occurring integral in Eq. (32) numerically for different K values which are in the regime discussed in Part I [1]. The resistivity as the function of the temperature is shown in Fig. 9 (a) and (b) for $S = 2$ and $S = 5/2$, respectively. The plots are similar to the experimental ones (see Sec. VII).

The effect of the anisotropy on the Kondo temperature defined by the largest slope in the resistivity can be examined by looking at the derivative of the calculated resistivity vs. temperature. We can see from Fig. 9 (a) and (b) that the Kondo temperature defined in that way is only slightly affected by the anisotropy in those cases where the Kondo effect is pronounced (e.g. $K < 0.5$ K in Fig. 9). The effect of the anisotropy becomes dominant for

larger strength of K . The temperature dependence of the resistivity has a maxima depending on the strength of K and the spin-flip contribution is freezing out gradually. That behavior is very different for integer and half-integer spins for large anisotropy. For integer spins the impurity contribution tends to zero in a way which is very sensitive on the strength of the anisotropy. In the case of half-integer spin the impurity resistivity approaching, however, a finite value at zero temperature which is independent of K . The resistivity there is determined by the dynamics of the two lowest energy levels shown in Fig. 2. In those cases the Kondo effect is also essentially reduced due to the smallness of the spin-flip amplitudes, but still presents. (The Kondo contribution in the lowest order is proportional to $\mathbf{S}\boldsymbol{\sigma}$ which gives a small amplitude for $M = \pm 1/2$.)

It is important to emphasize, that in case $S = 1/2$ the anisotropy is losing its meaning.

In a real system the anisotropy strength K has a distribution thus the formation of the resistivity maximum at finite value of temperature cannot be expected at least above the Kondo temperature. The calculation is anyhow not reliable for $T < T_K$.

VI. KONDO RESISTIVITY IN THIN FILMS

To get some information about the case of thin films a simple assumption is made that the two surfaces contribute to the anisotropy constant K in an additive way. The anisotropy factor for a sample with thickness t and in a distance d measured from one of the surface is

$$K(d, t) = K_d + K_{t-d} = \frac{\alpha}{d} + \frac{\alpha}{t-d} \quad (34)$$

where the coefficient α is estimated in Part I [1] (see Eq. (32)). The appropriate calculation of the resistivity including the elastic impurity scattering with mean free path l_{el} is a very difficult task for a film for an arbitrary ratio of l_{el}/t and value of K . In order to avoid those difficulties we are making use of the fact, that the magnetic exchange (Kondo) contribution to the resistivity ρ_{Kondo} is smaller by a factor 10^{-3} than the residual normal impurity resistivity ρ_{nor} ($\rho = \rho_{\text{nor}} + \rho_{\text{Kondo}}$), thus an expansion in the Kondo contribution is appropriate. The

calculation can be carried out in two limits (i) $t < l_{\text{el}}$ and (ii) $t \gg l_{\text{el}}$. It will be shown that the final expression does not depend on which limit is considered. In the case (i) the electrical resistivity contains the average value of the inverse electron life time. Denoting the resistivity at temperature T for a given value of K by $\rho(K, T)$, the average over the value of $K(d, t)$ is

$$\bar{\rho}(t, T) = \frac{1}{t} \int_0^t \rho(K(x, t), T) dx. \quad (35)$$

On the other hand, in case (ii) the sample can be considered as a set of parallel resistors of equal size, where each resistor represents a stripe in the sample with a constant K . In that case the conductances are additive, thus

$$\bar{\rho}(t, T) = \frac{1}{\sigma_{\text{nor}} + \frac{1}{N} \sum_i \sigma_i(K(x_i, t), T)} \quad (36)$$

where N is the number of the resistors (stripes) labeled by i and σ_i represents the Kondo conductivity of stripe i placed in distance x_i . In the actual case only the first stripes depend on the surface anisotropy. The Kondo conductivity is defined by the Kondo resistivity given by Eq. (32) as

$$\sigma = \sigma_{\text{nor}} + \sigma_{\text{Kondo}} = (\rho_{\text{nor}} + \rho_{\text{Kondo}})^{-1} \quad (37)$$

where $\sigma_{\text{Kondo}} \approx -\frac{\rho_{\text{Kondo}}}{\rho_{\text{nor}}^2} < 0$. The expansion gives the final expression

$$\bar{\rho}(t, T) = \rho_{\text{nor}} + \frac{1}{t} \int_0^t \rho_{\text{Kondo}}(K(x, t), T) dx. \quad (38)$$

That expression valid in the limit $\rho_{\text{Kondo}} \ll \rho_{\text{nor}}$ gives back exactly the expression in Eq. (35).

In the numerical calculation the integral in Eq. (35) or (38) is replaced by a weighted sum with appropriate intervals. Introducing the new integration variable d/α , the calculated Kondo resistivity depends only on t/α which is shown in Fig. 10 (a) and (b) for $S = 2$ and $S = 5/2$, respectively. Fitting the calculated Kondo resistivity for temperatures $T \gg T_K$ ($T = 2 - 4$ K) by the function $\rho_{\text{Kondo}}/\rho^{(0)} = -B_{\text{calc}} \ln T$ as it has been done in the

experimental works (see Sec. VII), the behavior of B_{calc} was examined as a function of t/α which can be seen in Fig. 11. To compare this calculated dependence of the coefficient B on the thickness to the experimental data, they were fitted by the function $B(t) = \rho^{(0)} B_{\text{calc}}(t/\alpha)$ as it is shown in Fig. 12. The fitted value of α is $\alpha = 247.7 \text{ \AA K}$ which is in agreement with the prediction given in Part I [1] by Eq. (32) (see Sec. VII). The fit is not too sensitive to small changes ($< 5\%$) in α .

If the sample is not thin, then the above results can be phenomenologically described in the framework of a simple model where the impurities in the region of the surface do not contribute to the Kondo resistivity and outside that region they are not affected. In this way the effective suppression length λ can be introduced and then the average resistivity at low temperature ρ_t e.g. for a thickness t

$$\rho_t = \rho_{t=\infty} \frac{t - 2\lambda}{t}. \quad (39)$$

According to this semi-phenomenological formula $B(t) = B_{\infty}(1 - 2\lambda/t)$ which was fitted to the experimental data. This can be seen also in Fig. 12 where the fitted value of the effective suppression layer parameter is $\lambda = 207.5 \text{ \AA}$.

The effect of the mean free path in the ballistic region can be demonstrated directly by taking into account the effect of the mean free path in the anisotropy constant. We calculated the change of the electrical resistivity for a thin film with thickness $L = 600 \text{ \AA}$ with anisotropy arising only at one of the surfaces in the forms

$$K = A \frac{\xi}{d} \quad (40a)$$

$$K = A \frac{\xi}{d} e^{-d/\xi} \quad (40b)$$

where ξ is the elastic mean free path (e.g. $\xi = 100 \text{ \AA}$), d is the distance measured from the surface with anisotropy of strength A , and the exponential decay is due to the mean free path. The electrical resistivity is calculated for $S = 2$ at $T = 2T_K$ just above the Kondo temperature T_K , as a function of the strength A of the anisotropy for two cases without and

with exponential factor (see Eq. (40)). Increasing the anisotropy strength A the spins are completely frozen in nearby the surface, but that region is limited by the finite mean free path. Fig. 13 clearly demonstrates that the strength of the anisotropy and the size of the suppression layer are reduced due to the finite mean free path as it is calculated by taking into account the anisotropy only for one of the surfaces.

VII. COMPARISON WITH EXPERIMENTS

In the last couple of years a very extensive study of the Kondo effect in thin films and wires have been performed. The experimental works were concentrating on determination of the effect of reduced dimensions on the Kondo temperature T_K and the amplitude of the resistivity anomaly. A detailed critical discussion of the earlier works are given in [10]. The early studies have been performed by Giordano and his collaborators [11,12], and by DiTusa, Lin, Park, Isaacson and Parpia [13]. In order to discuss the effect of uncoupled magnetic impurities, first only those experiments are listed which are performed in dilute limit, thus e.g. for Au(Fe) alloys the Fe concentration is 30 ppm. These experiments belong to two groups depending whether size effect was observed or not.

Concerning the theory two regions must be distinguished. When the size of the sample (e.g. the thickness of the sample) is inside the ballistic region, then obviously the present theory must be applied. In the case of thicker samples more care must be paid. There is another theory by Martin, Wan and Phillips [14] which is applicable in the opposite limit of weak localization, where the disorder-induced depression or enhancement of the Kondo effect is predicted depending on the value of the spin flip scattering rate τ_s^{-1} (depression is the case where $T_K, \hbar\tau_s^{-1} \ll T$). The competition between these theories needs further studies.

In the following the discussion is organized according to different effects. First we discuss how the change in the density of states at the surface can influence the Kondo effect, but it is ruled out as an explanation of the size effects to be discussed, because it is applicable only

on much smaller scale (Sec. VII A). Then the experiments with considerable dependence on the size of the samples are discussed and compared with the present theory (Sec. VII B). Finally those experiments are listed where no size effect was observed (Sec. VII C) or the concentrations of the impurities are in the spin glass region (Sec. VII D).

A. Density of states effects

As it has been discussed in Sec. I of Part I [1], the size dependence cannot be expected just because the Kondo cloud cannot fully develop in all directions by reducing the size of the sample. The only possibility which has been discussed by Zaránd [15] is, that nearby the surface there is a change in the density of states of conduction electrons by formation of a Friedel type oscillation due to the surface. That explanation was ruled out, because those changes in the density of states are very much localized in a few atomic distances measured from the surface and the smallest sizes in the experiments to be discussed are about 300\AA . That effect may, however, show up in point contact experiments where the contact size is smaller by even more than one order of magnitude. Such experiments were performed by Yanson and his collaborators [16–18] with Mn and Fe impurities in Cu contacts. Zaránd and Udvardi [19,20] showed that depending on the actual position of the impurity the density of states for an essential energy range around the Fermi surface can be enhanced or depressed by even 20%, thus $\rho = \rho_0 + \delta\rho$, where $|\delta\rho/\rho_0| < 0.2$. Just in order to demonstrate the effect an energy independent $\delta\rho$ is assumed and for that case in the expression of the Kondo temperature $\exp[-1/2J(\rho_0 + \delta\rho)] = \exp[-1/2J\rho_0] \exp[(2J\rho_0)^{-1} \frac{\delta\rho}{\rho_0}]$ there is an enhancement due to the second factor. Depending on the value of $(J\rho_0)^{-1}$ that enhancement can be over a factor of 100 for Mn and about 2 – 3 for Fe impurities. The enhancement is the larger the smaller the Kondo temperature T_K [16–18,20]. In the experiments the enhancement is the larger the smaller the contact size, thus to have large enhancement most of the impurities must be nearby the surface. Similar effect was also seen [21] in point contacts with presumable tunneling two-level systems (TLS) where an atom jumps between two positions

and the orbital Kondo effect is developed [22,23] by coupling the conduction electrons with different angular momenta to the TLS. As the typical size of the studied films and wires are much larger and such a dominating enhancement of the Kondo temperature has never been observed, therefore that explanation can be ruled out.

B. Experiments with observed size effect

Giordano and his collaborators (see for a review [10]) have performed a series of different experiments under different conditions where the size effect was observed but the changes in the Kondo temperature were almost negligible. The experiments of different type are listed below.

(i) Dependence on film thickness.

The film experiments with thickness $265\text{\AA} - 1800\text{\AA}$ were performed e.g. with 30 ppm Fe in Au, but similar results are obtained also for 100 ppm [11,12]. The resistivity was fitted by the formula

$$\rho(T) = \rho - B \ln(T) \quad (41)$$

where B is an adjustable parameter. It is well known for the Kondo systems that B is just not the result of the first non-vanishing third order perturbational result where B would be $B \sim J^3$, but it is the actual slope nearby or somewhat above the Kondo temperature (see for example [10]). In the actual experiments the temperature range $1.8 - 4$ K was studied while $T_K = 0.3$ K. The dependence of that coefficient B on thickness was plotted as shown in Fig. 12. The experimental results are fitted by the calculated dependence of B on the thickness with parameter $\alpha = 247.7\text{\AA}$ K and by the semi-phenomenological formula given by Eq. (39) with the effective suppression layer parameter value $\lambda = 207.5\text{\AA}$ in Fig. 12 [24,25]. That value of α is in agreement with the estimate given in Part I [1] by Eq. (32). There was not any signal for essential change in the Kondo temperature [10] in agreement with our theoretical result. It is

interesting to note that the estimated Kondo coherence length was about $3 \cdot 10^4 \text{\AA}$, much larger than the thickness of the sample. Similar experiments were performed with wires where more geometrical effects are expected, but the results are qualitatively similar but not identical. The simple semi-phenomenological formula given by Eq. (39) is not appropriate in those cases. Qualitatively very similar results are reported in [26] but there are quantitative differences very likely due to the sample preparation.

(ii) Kondo proximity effect.

A set of experiments [27,28] were performed where the film of dilute alloys is covered by a second layer of pure metal. The observation was, that in the case of a thin layer of dilute alloys with a significant suppression of the Kondo effect the covering by a second pure film results in partial recovery of that suppression. In Fig. 14 with the suppression layers indicated it is shown that the bilayer structure has a suppression layer only on one side of the film of dilute alloys, thus only one half of the suppression is expected. In order to verify the importance of the role of the spin-orbit interaction in the superimposed layer to complete the neighborhood of the impurity with a uniform spin-orbit coupling, we suggest experiments where the superimposed layer has negligible spin-orbit interaction (e.g. Al or Mg). In that case the boundary is changed, but the anisotropy should remain.

(iii) Kondo proximity effect with overlayers with different disorder.

It has been shown experimentally [29] that the Kondo resistivity suppression in a film of dilute alloys covered by a pure film but with different disorder depends on the disorder in the overlayer. It was found that the larger the disorder the smaller the recovery is. As it is discussed above if the thickness of the overlayer and the mean free path l_{el} in it are larger than the thickness of the suppression layer λ , then the depression takes place only on one side of the film of dilute alloys. On the other hand, if the pure overlayers contains disorder, then the electron entering that overlayer cannot bring

back information to the magnetic impurity by their momenta, as their momenta is changed in the overlayer (the overlayer is not in the ballistic regime). In these cases the reduction in the anisotropy is only partially developed as the surroundings of the impurity is not perfectly spherical in contrast to the case of overlayer with long mean free path.

C. Experiments without size effect

In contrast to the measurements discussed in VII B there is a series of experiments by Chandrasekhar *et al.* [30] where the size dependence was not found. The geometries of these experiments were different, the thickness of the sample t was kept the same ($t = 380\text{\AA}$), but the width of the stripes w was changed between $380 - 10^6\text{\AA}$ (see Fig. 15). After the correction due to the weak localization effects and due to electron-electron interaction no size dependence was claimed. On the basis of the present theory, for samples $t \ll w$ no size dependence is expected as the ratio of the volume of the suppression layers to the total volume is not changing. Where $t \sim w$ the anisotropy due to the geometry becomes more complicated, thus it is hard to make comparison with the present theory. On the other hand for $t \sim w$ the experimental points are somewhat falling off from the main averaged line, that, of course, may be due to experimental errors. According to the present theory the averaged Kondo resistivity for $w \gg t$ had to be smaller than the bulk resistivity, but it seems to be not the case [31].

Finally it should be mentioned that no size effect was observed studying $\text{La}_{1-x}\text{Ce}_x$ films where Ce has $S = 1/2$ for which no surface anisotropy is expected [32].

D. Higher concentration

There are several experiments [13,33] with higher impurity concentration. In these cases the impurity-impurity interaction mediated by the RKKY interaction competes with the Kondo effect. In another set of experiments [13] the thickness of the film were changed

in samples made of Cu with 1000 ppm Cr and it was found very similar depression of the Kondo effect described above in Sec. VII B. The wires with geometries similar to those discussed in Sec. VII C but with 2800 ppm impurities do not show dependence on the width d [33], but the overall amplitude is substantially SU-suppressed compared to the bulk, which was attributed to spin-glass effects.

VIII. CONCLUSION

In the present paper the influence of the spin-orbit induced surface anisotropy is studied on the Kondo effect in dilute magnetic alloys samples of finite size at least in one dimension. That anisotropy splits the energy levels for impurity spin $S > 1/2$. That anisotropy reduces as the bulk part of the sample is approached relatively slowly as $1/d$ where d is the distance of the impurity measured from the surface. That anisotropy occurs for samples of any shape, but for those cases further theories should be developed. The range where the anisotropy is relevant can be characterized by the suppression length λ introduced in Sec. VI, which is proportional to the strength of the anisotropy but limited by the mean free path of the electron as the anisotropy reflects the presence of the surface in the ballistic region nearby the impurity. Thus that suppression length cannot exceed a few hundred Å in accordance with the experiments discussed in Sec. VII B.

That anisotropy hinders the motion of the impurity spin S if $S > 1/2$ and the Kondo effect is affected in those regions of the samples where the anisotropy is not negligible relative to the Kondo temperature T_K . In order to calculate the Kondo resistivity the renormalized exchange coupling constants are calculated in Sec. III and IV by using the multiplicative renormalization group technique which is applicable only for temperatures T larger than the Kondo temperature T_K , thus no detailed prediction can be made outside that region. It can be accepted, however, that if the Kondo effect is already reduced in region $T > T_K$ similar effect is expected also for $T < T_K$. The resistivity is calculated by solving the Boltzmann equation in Sec. V for integer and half-integer spins with different anisotropy strength. Even

if the calculated resistivity curves in Fig. 9 (a) and (b) show different characteristic features by developing a resistivity maxima at different temperatures and of different amplitudes, those features are almost loosen as an average over the strength of the anisotropy is taken for $T > T_K$. The curves calculated for thin films (see Fig. 10) show smooth increase of the resistivity. More structures could be expected only in those experiments where the impurities are in certain distance measured from the surface. If the anisotropy does not dominate the complete sample then as the result of the average taken the largest resistivity slope as a function of temperature is in the region of the Kondo temperature T_K , and its position cannot be shifted too much on the scale of the Kondo temperature T_K . That theoretical result is in accordance with the experimental findings (see Sec. VII B).

The relatively weak sensitivity of the observed region of the largest resistivity slope on the size of the samples rules out the density states effects nearby the surface in contrast to the point contact experiments (see Sec. VII A). The size dependence associated with the large Kondo compensation cloud is not observed in agreement with the Kondo theory where such a simple connection is ruled out.

The calculated Kondo resistivity for thin films was fitted for temperatures $T \gg T_K$ ($T = 2 - 4$ K) by the function $\rho_{\text{Kondo}}/\rho^{(0)} = -B_{\text{calc}} \ln T$ which is compared to the experimental data in Fig. 12 and gives excellent agreement.

The phenomenological theory using the effective suppression length λ (see Sec. VI) works remarkable well to interpret qualitatively the experimental data quoted in Sec. VII. The fit of the experimental data is shown in Fig. 12.

The different proximity effects described in Sec. VII B can be also well explained by the present theory.

It is important that the role of mean free path (Sec. VI, see Fig. 13) reduces the effect of the large anisotropy constant, thus for a large range of strong anisotropy the size dependence remains in a limited range as far as the elastic mean free paths are in the same order of magnitude. In this way the size effect can be comparable for different host materials with different large spin-orbit interactions but with comparable elastic mean free path.

We have to emphasize, however, that our calculation does not consider the localization effects which are present in samples of larger sizes. Such effect have recently been predicted by Martin, Wan and Phillips [14] and deserves further detailed studies.

In addition to those localization effects the theoretical studies must be extended to the microscopic calculations of the anisotropy constant.

Considering further experiments the mean free path effects should be studied. The most relevant experiment to directly verify the role of the spin-orbit interaction could be the proximity experiments where the superimposed layer would be made of another metal without spin-orbit interaction as it is discussed in Sec. VII B. In those cases the uniform surrounding of the impurity would not be developed, thus the anisotropy remains. Furthermore, the experiments with impurities in a certain distance measured from the surface would be also very instructive.

Summarizing, the presented theory is able to provide a coherent description of the size effects of the Kondo resistivity in thin films, which is not related to the size of the Kondo compensation cloud in any sense.

ACKNOWLEDGMENT

The present authors are grateful for useful discussion with G. Bergmann, L. Borda, N. Giordano, B. L. Gyorffy, H. v. Löhneysen, Ph. Nozières, M. Parpia, P. Phillips, J. Sólyom, L. Szunyogh, I. K. Yanson and G. Zaránd. The work was supported by grants Hungarian OTKA T02228/1996 and T024005/1997. One of us (O.Ú.) was supported by TEMPUS Mobility Grant and A.Z. is grateful for the support by the Humboldt Foundation.

APPENDIX:

Here we calculate the second and third order vertex corrections, and the second order self-energy correction for the impurity spin shown in Fig. 5 and Fig. 6, respectively.

Carrying out the Matsubara's summation, analytical continuation, changing the integrals $\int \frac{d^3k}{(2\pi)^3}$ to $\int \rho(\varepsilon)d\varepsilon \int \frac{d\Omega_k}{4\pi}$ and using the assumption for $\rho(\varepsilon)$ in Section I, the contribution of the second order diagrams are

$$J_{MM''}J_{M''M'}(\sigma^i\sigma^j)_{\sigma\sigma'}S_{MM''}^iS_{M''M'}^j\rho_0\int_{-D}^D d\varepsilon\frac{1-n_F(\varepsilon)}{\varepsilon-\omega+K_{M''}-K_M} \\ +J_{MM''}J_{M''M'}(\sigma^j\sigma^i)_{\sigma\sigma'}S_{MM''}^iS_{M''M'}^j\rho_0\int_{-D}^D d\varepsilon\frac{n_F(\varepsilon)}{\varepsilon-\omega+K_{M'}-K_{M''}}, \quad (\text{A1})$$

for diagrams corresponding to Fig. 5 (a). The third order diagrams' contributions are

$$-(\sigma^i\sigma^j\sigma^k)_{\sigma\sigma'}J_{MN}J_{NN'}J_{N'M'}S_{MN}^iS_{NN'}^jS_{N'M'}^k\rho_0^2 \\ \cdot\int_{-D}^D\frac{(1-n_F(\varepsilon)d\varepsilon)}{\omega-\varepsilon+K_M-K_N}\int_{-D}^D\frac{(1-n_F(\varepsilon'))d\varepsilon'}{\omega-\varepsilon'+K_M-K_{N'}} \\ -(\sigma^k\sigma^j\sigma^i)_{\sigma\sigma'}J_{MN}J_{NN'}J_{N'M'}S_{MN}^iS_{NN'}^jS_{N'M'}^k\rho_0^2 \\ \cdot\int_{-D}^D\frac{n_F(\varepsilon)d\varepsilon}{\varepsilon-\omega+K_{M'}-K_N}\int_{-D}^D\frac{n_F(\varepsilon')d\varepsilon'}{\varepsilon'-\omega+K_{M'}-K_{N'}} \quad (\text{A2})$$

for diagrams corresponding Fig. 5 (b),

$$-Tr(\sigma^i\sigma^j)\sigma_{\sigma\sigma'}^k J_{MN}J_{NN'}J_{N'M'}S_{MN}^iS_{N'M'}^jS_{NN'}^k\rho_0^2 \\ \cdot\int_{-D}^D\int_{-D}^D\frac{n_F(\varepsilon)(1-n_F(\varepsilon'))d\varepsilon d\varepsilon'}{(\varepsilon-\varepsilon'+K_M-K_N)(\varepsilon-\varepsilon'+K_{M'}-K_{N'})} \quad (\text{A3})$$

for diagram Fig. 5 (c), and

$$(\sigma^i\sigma^j\sigma^k)_{\sigma\sigma'}J_{MN}J_{NN'}J_{N'M'}S_{MN}^jS_{NN'}^iS_{N'M'}^k\rho_0^2 \\ \cdot\int_{-D}^D\int_{-D}^D\frac{n_F(\varepsilon)(1-n_F(\varepsilon'))d\varepsilon d\varepsilon'}{(\omega-\varepsilon'+K_M-K_{N'})(\varepsilon-\varepsilon'+K_M-K_N)} \\ +(\sigma^k\sigma^j\sigma^i)_{\sigma\sigma'}J_{MN}J_{NN'}J_{N'M'}S_{MN}^jS_{NN'}^iS_{N'M'}^k\rho_0^2 \\ \cdot\int_{-D}^D\int_{-D}^D\frac{(1-n_F(\varepsilon))n_F(\varepsilon')d\varepsilon d\varepsilon'}{(\varepsilon'-\omega+K_{M'}-K_{N'})(\varepsilon'-\varepsilon+K_M-K_N)} \\ +(\sigma^i\sigma^j\sigma^k)_{\sigma\sigma'}J_{MN'}J_{N'N}J_{NM'}S_{MN}^iS_{NN'}^kS_{N'M'}^j\rho_0^2 \\ \cdot\int_{-D}^D\int_{-D}^D\frac{n_F(\varepsilon)(1-n_F(\varepsilon'))d\varepsilon d\varepsilon'}{(\omega-\varepsilon'+K_M-K_N)(\varepsilon-\varepsilon'+K_{M'}-K_{N'})} \\ +(\sigma^k\sigma^j\sigma^i)_{\sigma\sigma'}J_{MN'}J_{N'N}J_{NM'}S_{MN}^iS_{NN'}^kS_{N'M'}^j\rho_0^2$$

$$\cdot \int_{-D}^D \int_{-D}^D \frac{(1 - n_F(\varepsilon))n_F(\varepsilon')d\varepsilon d\varepsilon'}{(\varepsilon' - \omega + K_{M'} - K_N)(\varepsilon' - \varepsilon + K_{M'} - K_{N'})} \quad (\text{A4})$$

for diagrams corresponding Fig. 5 (d).

The second order correction to the self-energy for the impurity spin according to Fig. 6 is

$$- \text{Tr}(\sigma^i \sigma^j) J_{MM'} J_{M'M} S_{MM'}^i S_{M'M}^j \rho_0^2 \int_{-D}^D d\varepsilon \int_{-D}^D d\varepsilon' \frac{(1 - n_F(\varepsilon))n_F(\varepsilon')}{\varepsilon - \varepsilon' - \tilde{\omega} + K_{M'} - K_M}. \quad (\text{A5})$$

For the same indices summation must be carried out.

The spin factors in Eq. (A1), (A2), (A3), (A4) and (A5) were calculated by using the identities

$$(\sigma^i \sigma^j)_{\sigma\sigma'} = \delta_{ij} \delta_{\sigma\sigma'} + i\varepsilon_{ijk} \sigma_{\sigma\sigma'}^k, \quad (\text{A6a})$$

$$(\sigma^i \sigma^j \sigma^k)_{\sigma\sigma'} = \delta_{ij} \sigma_{\sigma\sigma'}^k + \delta_{jk} \sigma_{\sigma\sigma'}^i - \delta_{ik} \sigma_{\sigma\sigma'}^j + i\varepsilon_{ijk} \delta_{\sigma\sigma'}, \quad (\text{A6b})$$

introducing the S^\pm operators in a usual way, and exploiting that their matrix elements are

$$S_{MM'}^+ = p(S, M') \delta_{M, M'+1} = \sqrt{S(S+1) - M'(M'+1)} \delta_{M, M'+1} \quad (\text{A7a})$$

$$S_{MM'}^- = q(S, M') \delta_{M, M'-1} = \sqrt{S(S+1) - M'(M'-1)} \delta_{M, M'-1}. \quad (\text{A7b})$$

Turning to the integrals in Eq. (A1), (A2), (A3), (A4) and (A5), after changing the integration variable in integrals containing $(1 - n_F(\varepsilon))$ or $(1 - n_F(\varepsilon'))$, from ε (ε') to $-\varepsilon$ ($-\varepsilon'$) they were evaluated in logarithmic approximation. The integrals in Eq. (A1) give logarithmic contribution

$$\begin{aligned} I_{MM''}^{(1)}(D) &= \int_{-D}^D d\varepsilon \frac{n_F(\varepsilon)}{\varepsilon + \omega + K_M - K_{M''}} \\ &\approx \ln \left| \frac{\omega + K_M - K_{M''}}{D} \right| + I(\omega + K_M - K_{M''}), \end{aligned} \quad (\text{A8})$$

for $D > |\omega + K_M - K_{M''}|$ and

$$\begin{aligned}
I_{M'M''}^{(2)}(D) &= \int_{-D}^D d\varepsilon \frac{n_F(\varepsilon)}{\varepsilon - \omega + K_{M'} - K_{M''}} \\
&\approx \ln \left| \frac{\omega - K_{M'} + K_{M''}}{D} \right| + I(\omega - K_{M'} + K_{M''}),
\end{aligned} \tag{A9}$$

for $D > |-\omega + K_{M'} - K_{M''}|$.

The integral in Eq. (A5) gives logarithmic contribution

$$\begin{aligned}
I_{MM'}^{(3)}(D) &= \int_{-D}^D d\varepsilon \int_{-D}^D d\varepsilon' \frac{n_F(\varepsilon)n_F(\varepsilon')}{\varepsilon + \varepsilon' + \tilde{\omega} - \lambda + K_M - K_{M'}} \\
&\approx (\tilde{\omega} - \lambda + K_M - K_{M'}) \ln \left| \frac{\tilde{\omega} - \lambda + K_M - K_{M'}}{D} \right|,
\end{aligned} \tag{A10}$$

for $D > |\tilde{\omega} - \lambda + K_M - K_{M'}|$.

The integrals in Eq. (A2) give logarithmic contribution

$$\begin{aligned}
I_{MNN'}^{(4)}(D) &= I_{MN}^{(1)}(D) I_{MN'}^{(1)}(D) \\
&\approx \left(\ln \left| \frac{\omega + K_M - K_N}{D} \right| + I(\omega + K_M - K_N) \right) \\
&\quad \cdot \left(\ln \left| \frac{\omega + K_M - K_{N'}}{D} \right| + I(\omega + K_M - K_{N'}) \right)
\end{aligned} \tag{A11}$$

for $D > |\omega + K_M - K_N|$ and $D > |\omega + K_M - K_{N'}|$ and

$$\begin{aligned}
I_{M'NN'}^{(5)}(D) &= I_{M'N}^{(2)}(D) I_{M'N'}^{(2)}(D) \\
&\approx \left(\ln \left| \frac{\omega - K_{M'} - K_N}{D} \right| + I(-\omega + K_M - K_N) \right) \\
&\quad \cdot \left(\ln \left| \frac{\omega - K_{M'} - K_{N'}}{D} \right| + I(-\omega + K_{M'} - K_{N'}) \right)
\end{aligned} \tag{A12}$$

for $D > |-\omega + K_{M'} - K_N|$ and $D > |-\omega + K_M - K_{N'}|$.

The integral in Eq. (A3) gives logarithmic contribution for $M \neq N$, $M' \neq N'$ and $K_{M'} - K_{N'} - K_M + K_N \neq 0$

$$\begin{aligned}
I_{MNM'N'}^{(6)}(D) &= \int_{-D}^D d\varepsilon \int_{-D}^D d\varepsilon' \frac{n_F(\varepsilon)n_F(\varepsilon')}{(\varepsilon + \varepsilon' + K_M - K_N)(\varepsilon + \varepsilon' + K_{M'} - K_{N'})} \\
&\approx \frac{K_M - K_N}{K_{M'} - K_{N'} - K_M + K_N} \ln \left| \frac{K_M - K_N}{D} \right| \\
&\quad - \frac{K_{M'} - K_{N'}}{K_{M'} - K_{N'} - K_M + K_N} \ln \left| \frac{K_{M'} - K_{N'}}{D} \right|
\end{aligned} \tag{A13}$$

for $D > |K_M - K_N|$, $D > |K_{M'} - K_{N'}|$. For $K_{M'} - K_{N'} = K_M - K_N \neq 0$

$$I_{MNM'N'}^{(6)}(D) \approx -\ln \left| \frac{K_M - K_N}{D} \right|, \quad (\text{A14})$$

for $D > |K_M - K_N|$. And

$$I_{MMM'M'}^{(6)}(D) \approx -\ln \left| \frac{T}{D} \right|. \quad (\text{A15})$$

The integrals in Eq. (A4) give logarithmic contribution

$$\begin{aligned} I_{MN'MN}^{(7)}(D) &= \int_{-D}^D d\varepsilon \int_{-D}^D d\varepsilon' \frac{n_F(\varepsilon)n_F(\varepsilon')}{(\varepsilon' + \omega + K_M - K_{N'})(\varepsilon + \varepsilon' + K_M - K_N)} \\ &\approx \frac{1}{2} \ln^2 \left| \frac{\omega + K_M - K_{N'}}{D} \right| + I(\omega + K_M - K_{N'}) \ln \left| \frac{\sqrt{(K_M - K_N)^2 + T^2}}{D} \right|, \end{aligned} \quad (\text{A16})$$

for $D > |\omega + K_M - K_{N'}|$ and $D > \sqrt{(K_M - K_N)^2 + T^2}$, where T is the temperature,

$$\begin{aligned} I_{M'N'MN}^{(8)}(D) &= \int_{-D}^D d\varepsilon \int_{-D}^D d\varepsilon' \frac{n_F(\varepsilon)n_F(\varepsilon')}{(\varepsilon' - \omega + K_{M'} - K_{N'})(\varepsilon + \varepsilon' + K_M - K_N)} \\ &\approx \frac{1}{2} \ln^2 \left| \frac{-\omega + K_{M'} - K_{N'}}{D} \right| + I(-\omega + K_{M'} - K_{N'}) \ln \left| \frac{\sqrt{(K_M - K_N)^2 + T^2}}{D} \right|, \end{aligned} \quad (\text{A17})$$

for $D > |-\omega + K_{M'} - K_{N'}|$ and $D > \sqrt{(K_M - K_N)^2 + T^2}$,

$$\begin{aligned} I_{MNM'N'}^{(9)}(D) &= \int_{-D}^D d\varepsilon \int_{-D}^D d\varepsilon' \frac{n_F(\varepsilon)n_F(\varepsilon')}{(\varepsilon' - \omega + K_M - K_N)(\varepsilon + \varepsilon' + K_{M'} - K_{N'})} \\ &= I_{MNM'N'}^{(7)}(D), \end{aligned} \quad (\text{A18})$$

and

$$\begin{aligned} I_{M'NM'N'}^{(10)}(D) &= \int_{-D}^D d\varepsilon \int_{-D}^D d\varepsilon' \frac{n_F(\varepsilon)n_F(\varepsilon')}{(\varepsilon' - \omega + K_{M'} - K_N)(\varepsilon + \varepsilon' + K_{M'} - K_{N'})} \\ &= I_{M'NM'N'}^{(8)}(D). \end{aligned} \quad (\text{A19})$$

In the estimations above, the function $I(\alpha) = \int_0^\infty d\varepsilon n_F(\varepsilon) \frac{2\varepsilon}{\varepsilon^2 - \alpha^2}$ was introduced which is related to the finite T divergences. From the scaling equations the $I(\alpha)$ function is canceled out.

For the sake of handling these contributions more comfortable $\omega, \tilde{\omega} \sim T$ were set in the arguments of logarithms in a way that substituting $\omega + a$ ($\tilde{\omega} + a$) with $\sqrt{a^2 + T^2}$.

REFERENCES

- [1] see the preceding paper of O. Újsághy and A. Zawadowski, Phys. Rev. **B**.
- [2] O. Újsághy, A. Zawadowski, and B. L. Gyorffy, Phys. Rev. Lett. **76**, 2378 (1996).
- [3] O. Újsághy and A. Zawadowski, Proceedings of the *XXXIst Rencontres de Moriond*, Correlated fermions and transport in mesoscopic systems, Les Arcs, Savoie, France, January 20-27, 535 (1996).
- [4] Shin-ichi Kashiba *et al.*, Journal Phys. Soc. of Japan **55**, No. 4, 1341 (1986).
- [5] A. A. Abrikosov, Physics **2**, 5 (1965).
- [6] M. Fowler and A. Zawadowski, Solid State Commun. **9**, 471 (1971).
- [7] see for example A. A. Abrikosov, L. P. Gorkov, and I. E. Dzyaloshinski, *Methods of Quantum Field Theory in Statistical Physics*, (Dover Publications, Inc., New York).
- [8] J. Sólyom, J. Phys. **F 4**, 2269 (1974).
- [9] see, for example, Kei Yosida, Phys. Rev. **107**, 396 (1957).
- [10] M. A. Blachly and N. Giordano, Phys. Rev. **B 51**, 12537 (1995).
- [11] G. Chen and N. Giordano, Physica **B 165-166**, 455 (1990).
- [12] G. Chen and N. Giordano, Phys. Rev. Lett. **66**, 209 (1991).
- [13] J. F. DiTusa, K. Lin, M. Park, M. S. Isaacson, and M. Parpia, Phys. Rev. Lett. **68**, 1156 (1992).
- [14] I. Martin, Yi Wan, and Philip Phillips, Phys. Rev. Lett. **78**, 114 (1997).
- [15] G. Zaránd, Diploma Thesis at the Eotvos University of Budapest (1992), unpublished.
- [16] I. K. Yanson *et al.*, Sovjet Phys. Low. Temp. Phys. **20**, 1062 (1994).
- [17] I. K. Yanson, V. V. Fisun, R. Hesper, A. V. Khotkevich, J. M. Krams, J. A. Mydosh,

- and J. M. van Ruitenbeck, Phys. Rev. Lett. **74**, 302 (1995).
- [18] N. van der Post, F. L. Mettes, J. A. Mydosh, J. M. van Ruitenbeck, and I. K. Yanson, Phys. Rev. **B 53**, R 476 (1996).
- [19] G. Zaránd and L. Udvardi, Physica **B 218**, 68 (1996).
- [20] G. Zaránd and L. Udvardi, Phys. Rev. **B 54**, 7606 (1996).
- [21] R. J. Keijsers, O. I. Shklyarevskii, and H. van Kempen, Phys. Rev. **B 51**, 5628 (1995).
- [22] A. Zawadowski, Phys. Rev. Lett. **45**, 211 (1980).
- [23] see for a review D. Cox, A. Zawadowski cond-mat/9704103v2 (1997).
- [24] M. A. Blachly and N. Giordano, Phys. Rev. **B 46**, 2951 (1992).
- [25] M. A. Blachly and N. Giordano, Phys. Rev. **B 49**, 6788 (1994).
- [26] G. Apostolopoulos and C. Papastaikoudis, Solid State Comm. **99**, 277 (1996).
- [27] M. A. Blachly and N. Giordano, Physica **B 194-196**, 983 (1994).
- [28] M. A. Blachly and N. Giordano, Phys. Rev. **B 6788** (1994).
- [29] M. A. Blachly and N. Giordano, Europhys. Lett. **27**, 687 (1994).
- [30] V. Chandrasekhar, P. Santhanam, N. E. Penebe, R. A. Webb, H. Vloeberghs, C. H. Van Haesendock, and Y. Bruynseraede, Phys. Rev. Lett. **72**, 205 (1994).
- [31] V. Chandrasekhar, private communications
- [32] C. Roth, C. Sürgersand and H. v. Löhneysen, Phys. Rev. **B 54**, 534 (1996).
- [33] G. Neuttiens *et al.*, Europhys. Lett. (1997).

FIGURES

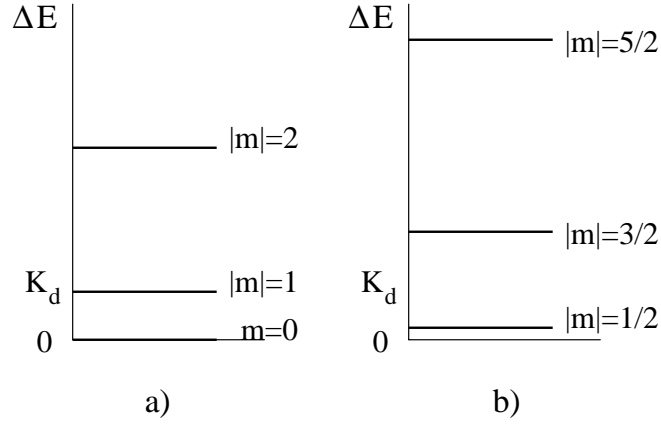


FIG. 1. The splitting schema due to the anisotropy for (a) $S = 2$ and (b) $S = 5/2$.

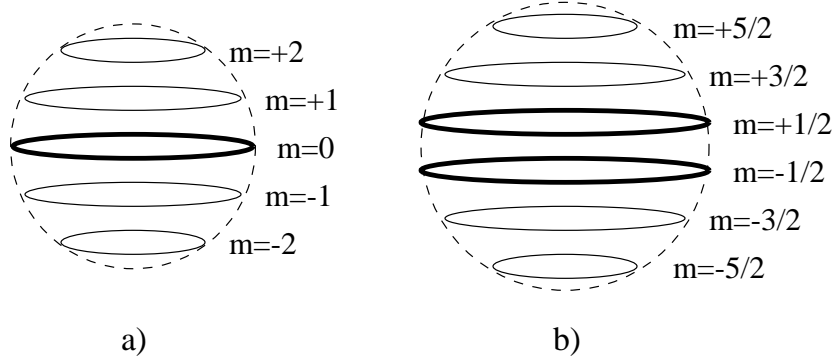


FIG. 2. The squizing of the spin into planar states due to the anisotropy is illustrated for (a) $S = 2$ and (b) $S = 5/2$. The lowest energy states are shown by heavy lines.

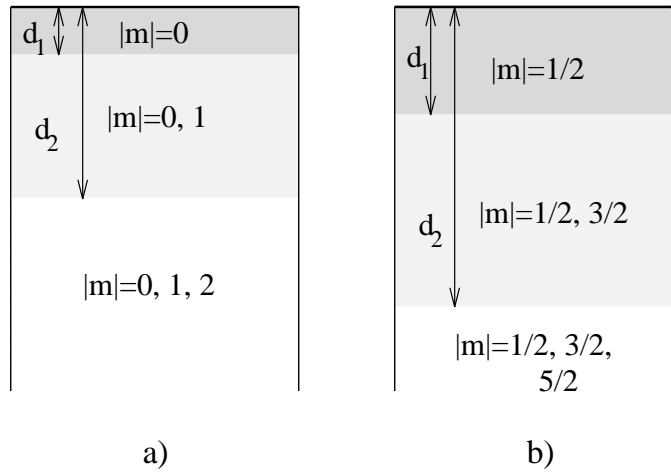


FIG. 3. The different layers of the impurity positions where more orbitals become active as the impurity positions approach the bulk assuming that $d_1, d_2 < l_{el}$. (a) $S = 2$, (b) $S = 5/2$.

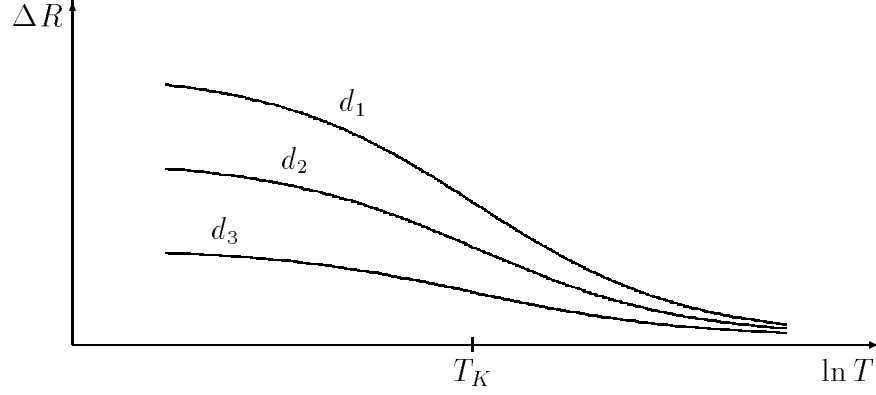


FIG. 4. The schematic plots of the contribution to the Kondo resistivity for impurities with different distances $d_3 < d_2 < d_1$ measured from the surface.

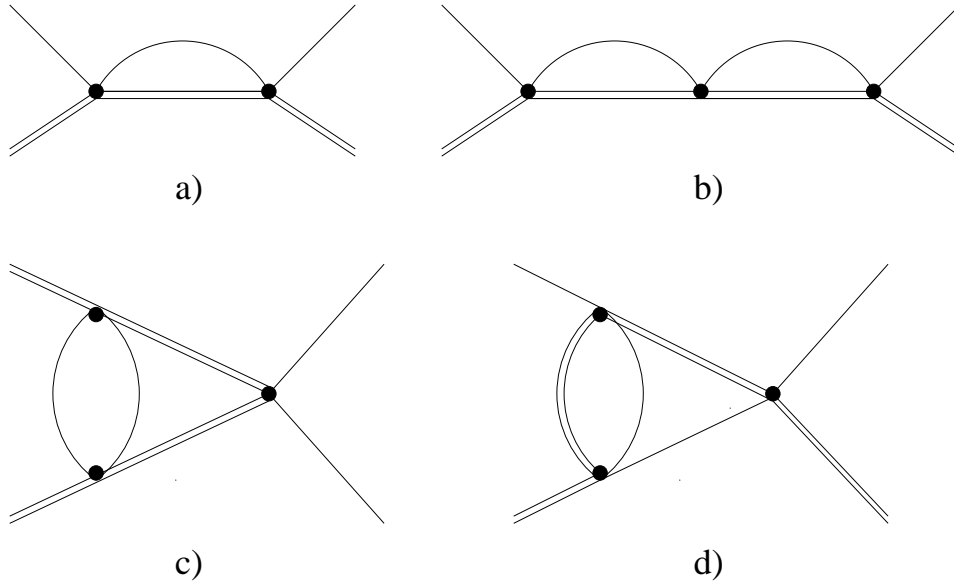


FIG. 5. The second and third order vertex corrections. The double line represents the impurity spin with the anisotropy energy, the single one the conduction electrons, and the solid circles stand for the exchange interaction.

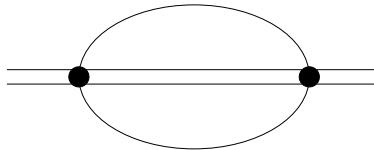


FIG. 6. The second order self-energy correction for the impurity spin. The double line represents the impurity spin with the anisotropy energy, the single one the conduction electrons, and the solid circles stand for the exchange interaction.

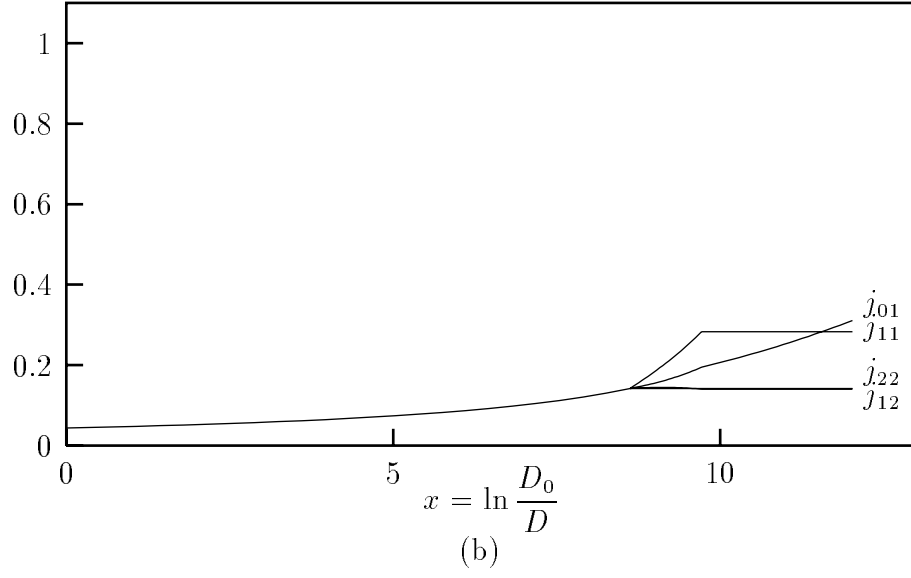
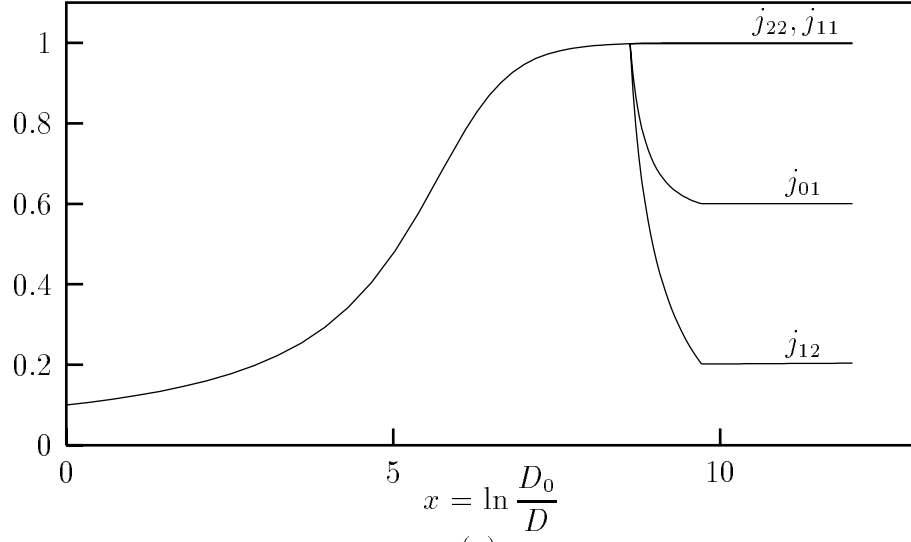


FIG. 7. The running couplings for $S = 2$ as a function of $x = \ln \frac{D_0}{D}$ at $K = 6$ K, $T = 0.6$ K with parameters $D_0 = 10^5 K$ and (a) $j_0 = 0.1$ (b) $j_0 = 0.0435$.

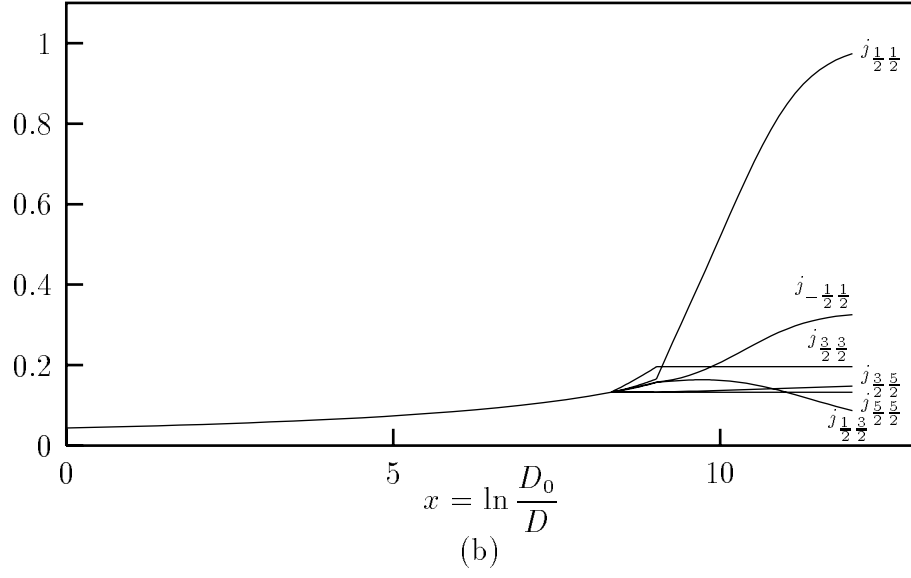
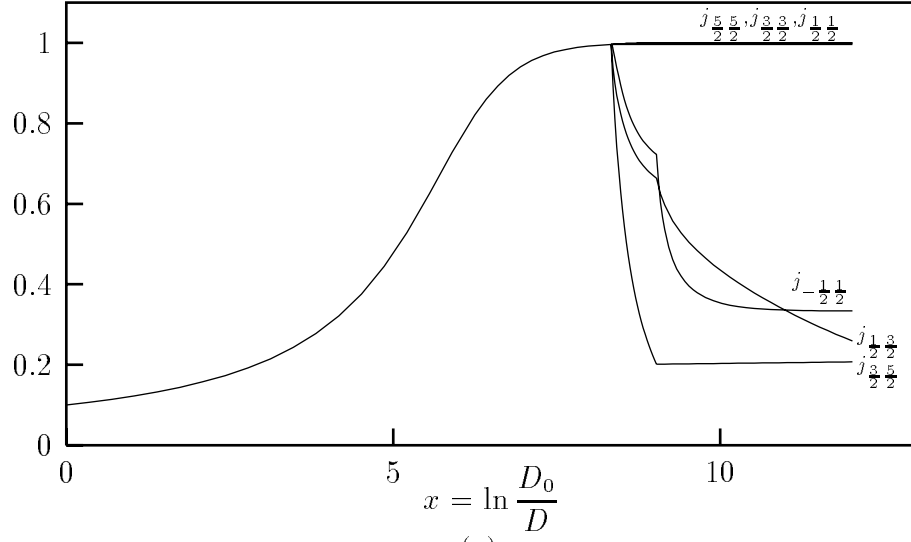


FIG. 8. The running couplings for $S = 5/2$ as a function of $x = \ln \frac{D_0}{D}$ at $K = 6$ K, $T = 0.6$ K with parameters $D_0 = 10^5$ K and (a) $j_0 = 0.1$ (b) $j_0 = 0.0435$.

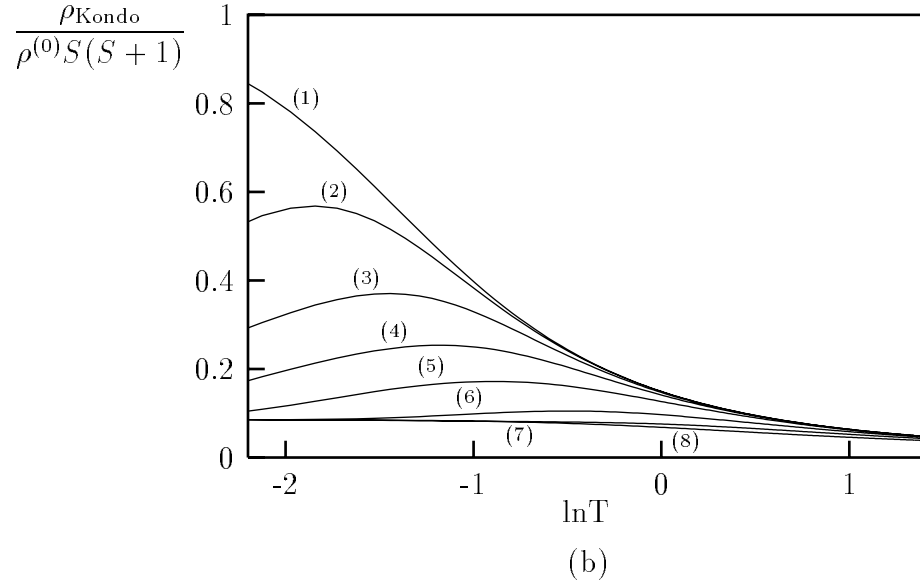
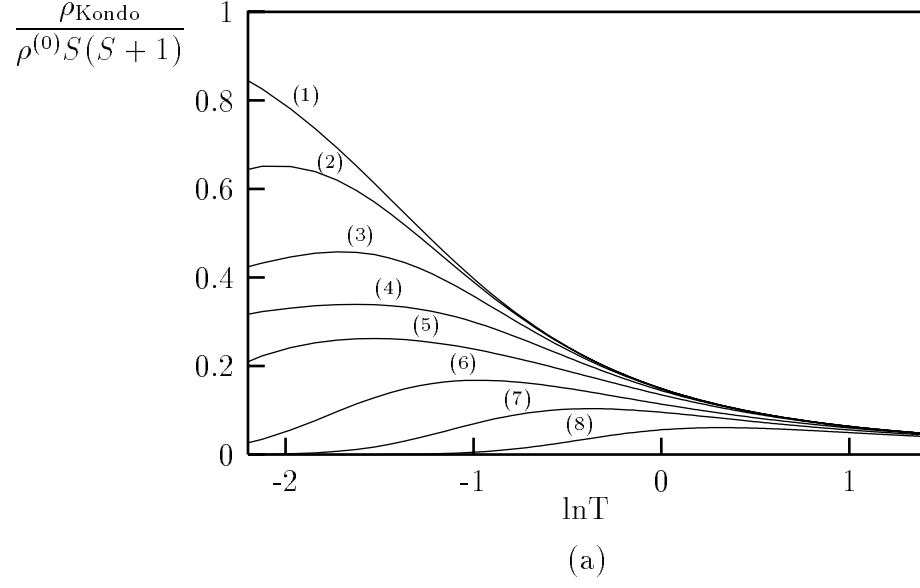


FIG. 9. The resistivity for (a) $S = 2$ and (b) $S = 5/2$ for different values of K . (1) $K = 0$ (2) $K = 0.02$ K (3) $K = 0.05$ K (4) $K = 0.1$ K (5) $K = 0.2$ K (6) $K = 0.5$ K (7) $K = 1$ K (8) $K = 2$ K. The initial parameters were chosen as $j_0 = 0.0435$ and $D_0 = 10^5$ K, $T_K = 0.3$ K.

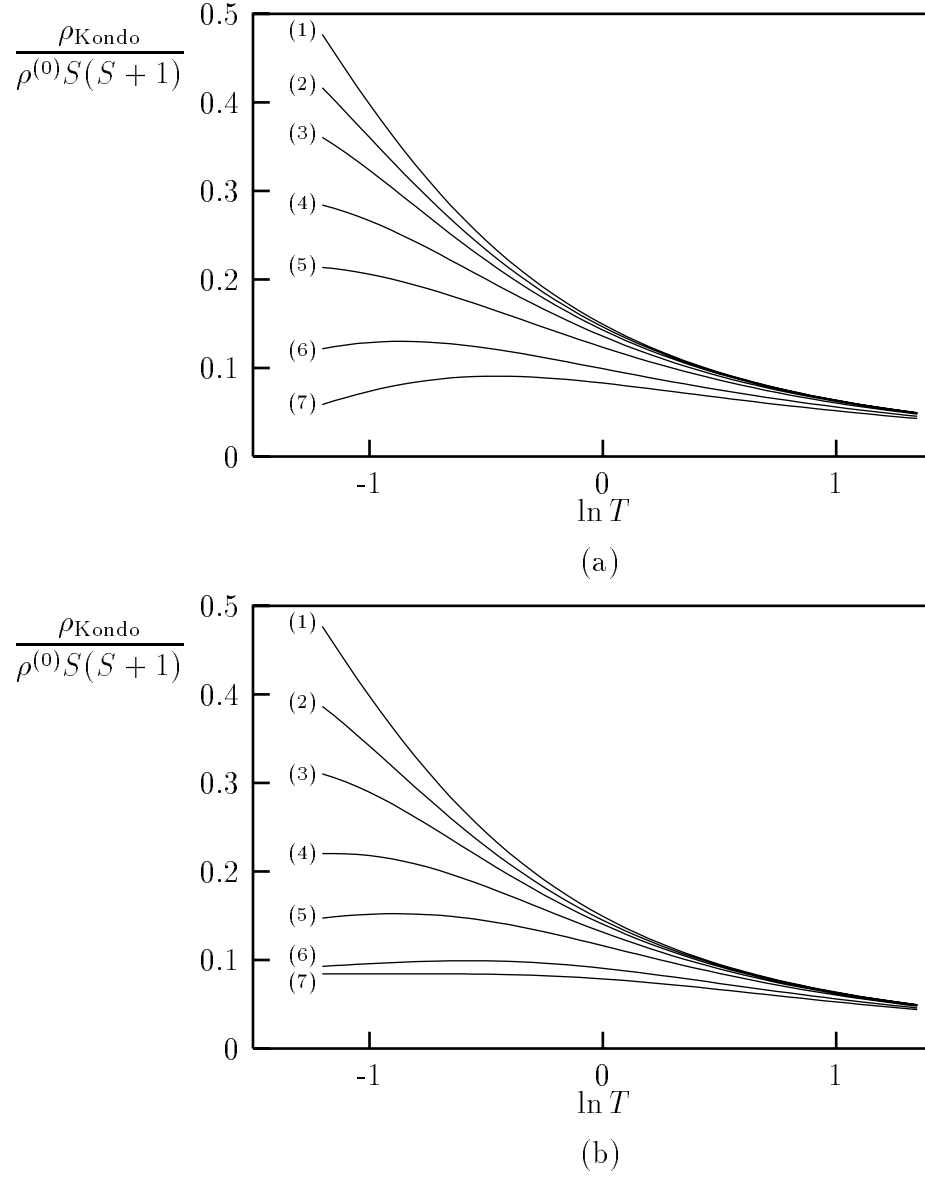


FIG. 10. The resistivity for (a) $S = 2$ and (b) $S = 5/2$ for different values of t/α . (1) $t/\alpha = \infty (K = 0)$ (2) $t/\alpha = 200 \frac{1}{K}$ (3) $t/\alpha = 100 \frac{1}{K}$ (4) $t/\alpha = 50 \frac{1}{K}$ (5) $t/\alpha = 25 \frac{1}{K}$ (6) $t/\alpha = 10 \frac{1}{K}$ (7) $t/\alpha = 6 \frac{1}{K}$. The initial parameters were chosen as $j_0 = 0.0435$ and $D_0 = 10^5$ K, $T_K = 0.3$ K.

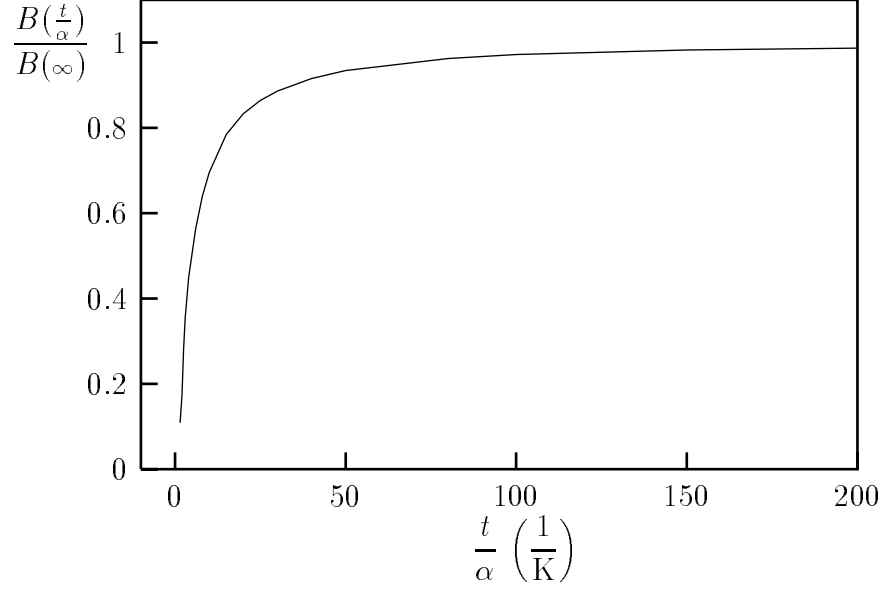


FIG. 11. The calculated coefficient B as a function of t/α . The Kondo temperature was chosen as $T_K = 0.3$ K.

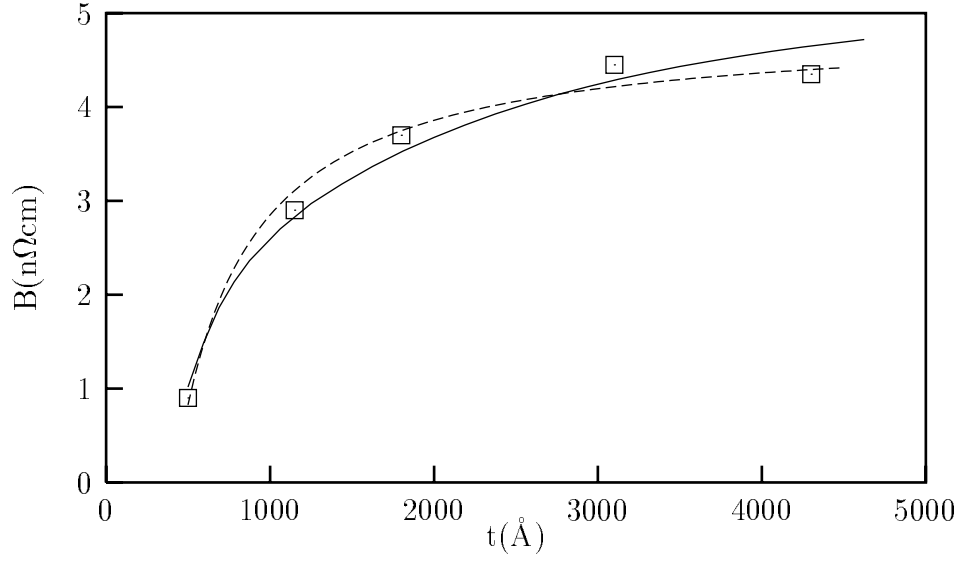


FIG. 12. Fit on the experimental data (squares) by the calculated formula $B(t) = \rho^{(0)} B_{\text{calc}}(t/\alpha)$ (the Kondo temperature was chosen as $T_K = 0.3$ K) with fitting parameters $\rho^{(0)} = 20 \text{ n}\Omega\text{cm}$, $\alpha = 247.7 \text{ \AA}$ K (solid line) and by the phenomenological theory $B(t) = B_{\infty}(1 - 2\lambda/t)$ with fitting parameters $B_{\infty} = 4.87 \text{ n}\Omega\text{cm}$, $\lambda = 207.5 \text{ \AA}$ (dashed line). The fit is not too sensitive to small changes ($< 5\%$) in α .

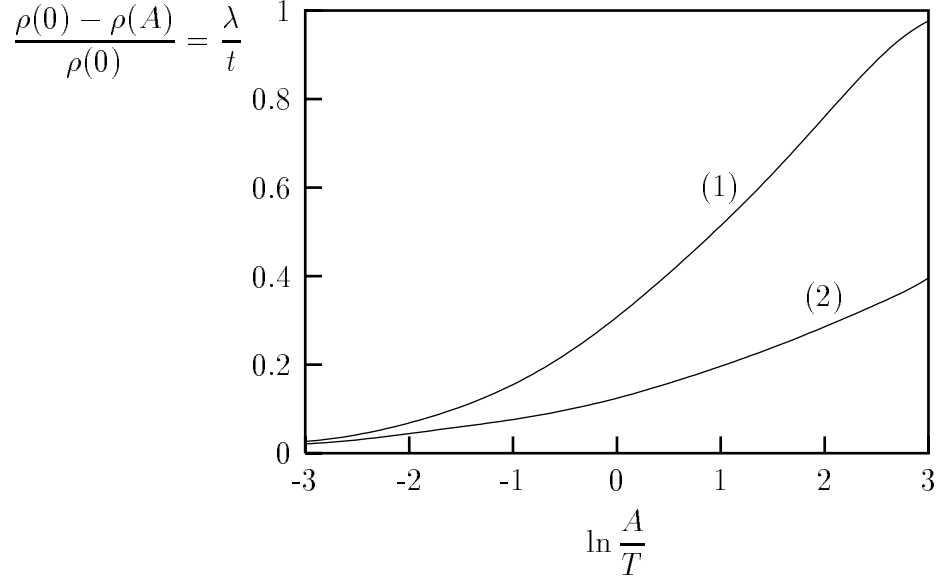


FIG. 13. The effect of the mean free path on the Kondo resistivity in the presence of anisotropy arising only one of the surface in a thin film with thickness $L = 600\text{\AA}$ for $S = 2$ at $T = 0.6\text{ K}$ (1) $K = A_d^\xi$ (2) $K = A_d^\xi e^{-d/\xi}$. The Kondo temperature was chosen as $T_K = 0.3\text{ K}$.

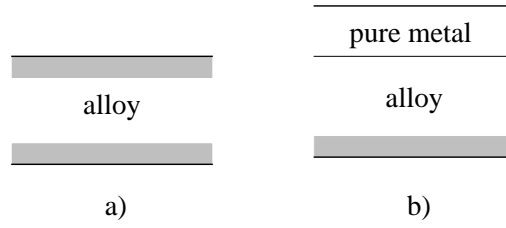


FIG. 14. Bilayer structure

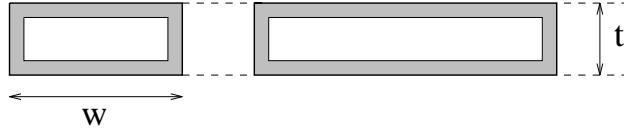


FIG. 15. Stripes with same thickness t and changing width w .